Journal of Catalysis **208,** 197–210 (2002)
doi:10.1006/jcat.2002.3555, available online at http://www.idealibrary.com on IDEAL®

Amorphous Vanadium Phosphate Catalysts Prepared Using Precipitation with Supercritical CO_2 as an Antisolvent

Graham J. Hutchings,*,[1] J. Antonio Lopez-Sanchez,* Jonathan K. Bartley,* Jeremy M. Webster,† Andrew Burrows,‡ Christopher J. Kiely,§ Albert F. Carley,* Colin Rhodes,* Michael Hävecker,¶ Axel Knop-Gericke,¶ Ralf W. Mayer,¶ Robert Schlögl,¶ Jean Claude Volta,‖ and Martyn Poliakoff†

*Department of Chemistry, Cardiff University, P.O. Box 912, Cardiff CF10 3TB, United Kingdom; †School of Chemistry, University of Nottingham, University Park, Nottingham NG7 2RD, United Kingdom; ‡Departments of Engineering and Chemistry, University of Liverpool, Liverpool L69 3BX, United Kingdom; §Department of Engineering, Materials Science and Engineering, University of Liverpool, Liverpool L69 3BX, United Kingdom; ¶Fritz-Haber-Institut der Max-Planck-Gesellschaft, Department of Inorganic Chemistry, Faradayweg 4-6, D-14195 Berlin (Dahlem), Germany; and ‖Institut de Recherches sur la Catalyse, CNRS, 2 Avenue Albert Einstein, 69626 Villeurbanne Cedex, France

Received November 19, 2001; revised February 1, 2002; accepted February 6, 2002

A new preparative route for vanadium phosphate catalysts is described using supercritical CO_2 as an antisolvent. The amorphous microspheroidal VPO produced is shown to be more active than comparable crystalline VPO catalysts for the selective oxidation of *n*-butane to maleic anhydride and, furthermore, does not require an extensive pretreatment or activation period to establish full catalytic activity. VPO catalysts prepared using supercritical CO_2 as an antisolvent maintain their amorphous nature throughout the catalyst test period. In contrast, amorphous VPO catalysts can also be prepared by using liquid CO_2 as antisolvent or by solvent evaporation *in vacuo*; however, these materials are found to partially crystallise during the oxidation of *n*-butane. The wholly amorphous catalysts are characterised using transmission electron microscopy, X-ray absorption spectroscopy, ^{31}P spin-echo mapping, NMR spectroscopy, and X-ray photoelectron spectroscopy. The role of amorphous material in vanadium phosphate catalysis is discussed in detail.

Key Words: ***n*-butane oxidation to maleic anhydride; amorphous and crystalline vanadium phosphates; antisolvent precipitation using supercritical CO_2.**

INTRODUCTION

Vanadium phosphate compounds are (utilised commercially as catalysts for the synthesis of maleic anhydride by the partial oxidation of *n*-butane. Consequently, vanadium phosphate catalysts have been extensively studied (1–4). The current commercial catalysts are prepared from *in situ* activation (5) of $VOHPO_4 \cdot 0.5H_2O$ under reaction conditions (6, 7). The resulting catalyst comprises a complex mixture of $(VO)_2P_2O_7$ in combination with α_{II}- and δ-$VOPO_4$ phases (6). Some researchers favour V^{4+} phases, e.g., $(VO)_2P_2O_7$ as the sole active phase (8–11). However, *in situ* Raman spectroscopy (5) suggests that combinations of V^{4+} and V^{5+} phases are required for the catalyst to exhibit high activity and selectivity to maleic anhydride. Indeed, Coulston *et al*. recently (12) showed that the presence of V^{5+} appears to be essential for the initial activation of *n*-butane, an observation that is essentially in agreement with earlier TAP pulse reactor experiments (13). To some extent, the debate concerning the involvement of specific VPO phases is complicated by the observation that many vanadium phosphate catalysts contain significant amounts of disordered material (5, 6, 9–11, 14–29). Some studies suggest that the amorphous material is an active component (5, 6, 15, 18, 19, 26–29), whereas others consider this not to be the case (8–11, 22). Amorphous VPO compounds have been used as one way to secure *in situ* regeneration in industrial reactors (30) by using a high-temperature treatment with pure *n*-butane. Indeed, the transformation of the crystalline precursor $VOHPO_4 \cdot 0.5H_2O$ to the crystalline catalyst $(VO)_2P_2O_7$ is observed to involve the transformation of significant amounts of amorphous material (6). Until recently, VPO catalysts containing solely amorphous material have not been investigated as active catalysts. In our earlier communication (31), we presented our initial results showing that an amorphous vanadium phosphate could be generated from precipitation using supercritical CO_2 as an antisolvent. In this paper, we extend these initial results and discuss the potential role of amorphous vanadium phosphate catalysts for the partial oxidation of *n*-butane.

EXPERIMENTAL

Catalyst Preparation

Preparation of crystalline $VOHPO_4 \cdot 0.5H_2O$. The hemihydrate $VOHPO_4 \cdot 0.5H_2O$ was prepared using three distinct routes, denoted VPA, VPO, and VPD. The *VPA hemihydrate* was prepared by dissolving V_2O_5 (6.06 g, Strem) in

[1] To whom correspondence should be addressed. E-mail: hutch@cardiff.ac.uk.

0021-9517/02 $35.00

aqueous HCl (35%, 79 ml) at reflux for 2 h. H_3PO_4 (8.91 g, 85%, Aldrich) was added, and the solution was refluxed for a further 2 h and subsequently evaporated to dryness. The resulting solid was refluxed in water (20 ml H_2O/g solid) for 1 h, filtered hot, washed with warm water, and then dried in air (110°C, 16 h).

The *VPO hemihydrate* was prepared by refluxing V_2O_5 (11.8 g, Strem) with H_3PO_4 (16.49 g, 85% Aldrich) in isobutanol (250 ml) for 16 h. The light blue solid was recovered by filtration, washed with isobutanol (200 ml) and ethanol (150 ml, 100%), refluxed in water (9 ml H_2O/g solid) for 1 h, filtered hot, and dried in air (110°C, 16 h).

The *VPD hemihydrate* was prepared from the dihydrate compound $VOPO_4 \cdot 2H_2O$. V_2O_5 (5.0 g, Strem) and H_3PO_4 (30 ml, 85%, Aldrich) were refluxed in water (120 ml) for 24 h. The yellow solid (yield 50% based on V) was recovered by vacuum filtration, washed with cold water (100 ml) and acetone (100 ml), and dried in air (110°C, 24 h). Powder X-ray diffraction and laser Raman spectroscopy confirmed that this solid was $VOPO_4 \cdot 2H_2O$. This $VOPO_4 \cdot 2H_2O$ phase (4 g) was refluxed with isobutanol (80 ml) for 21 h, and the resulting hemihydrate was recovered by filtration and dried in air (110°C, 16 h).

Catalyst preparation using supercritical CO_2 as an antisolvent. A solution of H_3PO_4 (1.8 g, 100%, Aldrich) in isopropanol (120 ml) was refluxed with $VOCl_3$ (1.6 ml, Aldrich) for 16 h to give a blue solution. The resulting isopropanol solution was processed using supercritical CO_2 to precipitate a vanadium phosphate using the apparatus shown schematically in Fig. 1 with the following methodology. The isopropanol solution was pumped through a fine capillary (220-μm i.d.) into a precipitation vessel containing concurrently flowing CO_2. The CO_2 can act as an effective antisolvent when it is either a liquid (>42 bar at 20°C) or a supercritical fluid ($T_c = 31.3$°C, $P_c = 72$ bar). CO_2 was pumped as a liquid using a modified HPLC pump at pressures of up to 110 bar. The system pressure was maintained by a back pressure regulator (BPR), and flow rates of the CO_2 and isopropanol solution could be set independently. To achieve supercritical conditions, the precipitation vessel (PV) was held in a GC oven, allowing control of the temperature from ambient to ca. 100°C. The CO_2 passed through a length of coiled tubing in the oven and was heated through its critical point, becoming supercritical. As the vanadium phosphate solution exited the capillary, the alcohol and CO_2 diffused into each other, causing the isopropanol to expand, hence reducing its solvent power. The higher temperature together with the removal of the organic solvent enabled rapid precipitation of the vanadium phosphate. The catalyst precursor denoted VPO_{SCP} was collected on a filter bed. The isopropanol solution was pumped at 0.1 ml/min through the capillary along with excess CO_2, which was pumped at 7 ml/min. The system pressure was held constant at 110 bar, and the precipitation vessel was maintained at 60°C. Experiments were typically conducted for 3 h which resulted in the synthesis of 0.2 g of solid. Similar experiments were conducted using isobutanol as the alcohol solvent, since this was the alcohol typically used in the conventional synthesis of $VOHPO_4 \cdot 0.5H_2O$ (32). A catalyst was also prepared using the same methodology but using liquid CO_2 ($P_{CO_2} = 60$ bar) at 15°C.

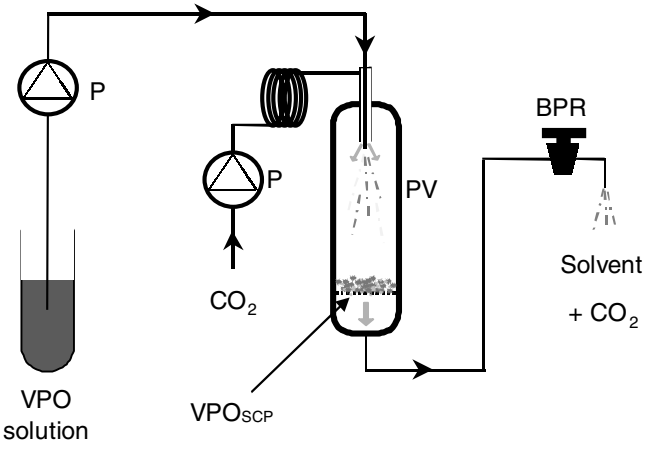

FIG. 1. Schematic of the apparatus for the precipitation of vanadium phosphates using either supercritical or liquid CO_2. BPR, back pressure regulator; PV, precipitation vessel; P, pumps.

Two further catalysts were prepared using similar methodologies. First a Co-containing catalyst was prepared using supercritical CO_2 precipitation for a modified solution containing 1 mol% Co. Cobalt has been previously identified as a promising promoter element for vanadium phosphate catalysts (4). More specifically, cobalt acetylacetonate (0.0288 g, Aldrich) was dissolved in the isopropanol vanadium phosphate solution previously described (100 ml), and the resulting solution was refluxed for 5 h. This solution was then processed using supercritical CO_2 as described previously. Second, a solution was prepared by adding acetylacetone (0.084 g, Aldrich) to the isopropanol vanadium phosphate solution (250 ml), and the resulting solution was refluxed for 5 h, prior to being processed using supercritical CO_2 as described above.

The attempts to obtain a solid from the standard isopropanol vanadium phosphate solution by solvent removal using distillation were unsuccessful. However, slow evaporation at 60°C under vacuum using a Schlenk line did lead to the formation of a solid which was also investigated as a potential catalyst.

Catalyst Testing

The oxidation of *n*-butane was carried out using a microreactor with a standard mass of catalyst (0.5 g). *n*-Butane and air were fed to the reactor via calibrated mass flow controllers to give a feedstock composition of 1.5% *n*-butane in air. The products were then fed via heated lines to an

online gas chromatograph for product analysis. The reactor comprised a stainless steel tube with the catalyst held in place by plugs of quartz wool. A thermocouple was located in the centre of the catalyst bed, and temperature control was typically $\pm 1^{\circ}$C. Carbon mass balances of $\geq 97\%$ were typically observed. Catalyst precursors were heated *in situ* (1.5% *n*-butane in air) at 400°C by heating the sample from room temperature at a rate of 3°C/min.

Catalyst Characterisation

A number of techniques were used to characterise the catalyst structure. Powder X-ray diffraction (XRD) was performed using an Enraf Nonius FRS90 X-ray generator with a Cu$K\alpha$ source fitted with an Inel CPS 120 hemispherical detector. BET surface area measurements using nitrogen adsorption were carried out using a Micromeritics ASAP 2000 instrument. Raman spectra were obtained using a Renishaw Ramanscope spectrograph fitted with a green Ar^+ laser ($\lambda = 514.532$ nm).

Scanning electron microscopy (SEM) was performed on a Hitachi S26YO-N instrument operating at 20 kV and fitted with a Link Systems EDX spectrometer. Transmission electron microscopy (TEM) observations were made with a JEOL 2000 EX high-resolution electron microscope operating at 200 kV. The instrument had been fitted with a low-light level TV camera and a frame-averaging system to allow the use of very low illumination conditions. This latter condition was essential for studying these beam-sensitive vanadium phosphorus oxide compounds. Samples suitable for TEM analysis were prepared by dispersing the catalyst powder onto a lacy carbon film supported on a copper-mesh grid.

The ^{31}P NMR measurements were performed on a Bruker MSL 300 NMR spectrometer. The ^{31}P spin–echo mapping method was shown by Li *et al.* (33) and Sananes *et al.* (34) to be a very powerful technique for evaluating the relative proportion of V^{5+} and V^{4+} ions surrounding the P atoms in vanadium phosphate compounds independent of the crystallinity. The ^{31}P NMR spin–echo spectra were recorded under static conditions, using a $90^{\circ}x$–τ–$180^{\circ}y$–τ acquisition sequence. The 90° probe duration was 4.2 μs and τ was 20 μs. For each sample, the irradiation frequency was varied in increments of 100 kHz above and below the ^{31}P resonance of H_3PO_4. The number of spectra recorded was dictated by the frequency limits beyond which no spectral intensity was detectable. The ^{31}P NMR spin–echo mapping information was then obtained by superposition of all the spectra.

X-ray photoelectron spectroscopy (XPS) was used to determine the P/V surface atomic ratio of the catalysts. XPS measurements were made using a VG ESCA 3 photoelectron spectrometer employing an Al$K\alpha$ X-ray source operating at 400 W. Samples were mounted using double-sided adhesive tape. Binding energies were referenced to the C 1*s* peak at 285 eV, and P : V ratios were calculated using the relative sensitivity factors (35).

X-ray absorption spectroscopy (XAS) in the soft energy range between 100 and 1000 eV represents a surface-sensitive method if applied in the electron yield mode. Complementary to photoelectron spectroscopy, XAS probes the unoccupied states. The spectra can be correlated more or less directly to the unoccupied density of states (DOS). Since the process is local and governed by dipole selection rules, the data are related to the site- and symmetry-selected DOS. No long-range order is necessary, and the method is therefore extremely useful for characterising amorphous material. For a long period, XAS was used solely under UHV conditions; however, we have developed a new setup which allows the collection of X-ray absorption data in the total electron yield mode under relatively high-pressure conditions (pressure = 2 mbar). This renders it possible to study the surface of a catalyst *in situ*, i.e., under conditions that are similar to normal working conditions.

The XAS experiments were performed with a special reactor cell consisting of two stainless-steel chambers. Details about the setup and the data processing can be found in the literature (36, 37). Experiments were carried out on the undulator beamline UE/56-2 at the third-generation Berliner Synchrotron Radiation Facility BESSY II (38). The near-edge X-ray absorption fine structure (NEXAFS) was analysed, i.e., the strong variations of the absorption coefficient just at the absorption edge. For the *in situ* experiments, a continuous flow of 1.5 vol% *n*-butane in both He and oxygen was dosed via two calibrated mass flow controllers at a total mass flow of 17.5 ml/min. The partial pressures of the *n*-C_4H_{10}/He mixture and the oxygen were 1.6 and 0.4 mbar, respectively, resulting in a total pressure in the reactor of 2 mbar during the NEXAFS measurements. The sample was heated in the reaction mixture by a resistive heater up to 400°C. The catalyst powder (50 mg) was pressed into a flat pellet (diameter, 13-mm) to mount it on the stainless steel sample holder. Part of the gas phase in the reactor was sampled via a capillary (diameter, 3-mm) just above the sample and analysed with a quadrupole mass spectrometer. The photon energy of the NEXAFS spectra was calibrated by the π^*-resonance of molecular oxygen at 530.8 eV. The resolving power $E/\Delta E$ was about 3000. Vanadium L_3-edge spectra were analysed by a least-squares fit applying Gauss–Lorentz profiles considering experimental and intrinsic broadening.

RESULTS

Catalyst Evaluation

A series of vanadium phosphate catalyst precursors were prepared from the isopropanol vanadium phosphate solution using the following methods: (i) precipitation with supercritical CO_2, (ii) precipitation with liquid CO_2, and

TABLE 1

Catalytic Activity of Vanadium Phosphate Catalysts

Preparation route	Maleic anhydride selectivity (%)[a]		Surface area ($m^2\ g^{-1}$)	Intrinsic activity[b] (mol MA $m^{-2}\ h^{-1}$)
	S_{10}^{MA}	S_{20}^{MA}		
VPA	68	52	4	2.8×10^{-5}
VPO	85	72	14	2.7×10^{-5}
VPD	70	68	43	2.4×10^{-5}
VPO_{SCP1}	—	45	4	4.6×10^{-5}
VPO_{SCP2}	—	42	3	0.42×10^{-5}
VPO_{LP}	—	39	6	2.9×10^{-5}
VPO_{EP}	42	—	8	1.7×10^{-5}
VPO_{CoSC}	28[c]	28	5	1.0×10^{-5}
VPO_{acacSC}	37	37	9	2.0×10^{-5}

[a] 5_{10}^{MA} and 5_{20}^{MA} = maleic anhydride selectivity at 10 and 20% conversion, respectively.

[b] GHSV = 2400 h^{-1} for VPA, VPO, VPD, VPO_{SCP1}, VPO_{LP}, and VPO_{EP} catalysts; 3000 h^{-1} for VPO_{SCP2}; and 4070 h^{-1} for VPO_{CoSC} and VPO_{acacSC} catalysts. The reaction temperature was 400°C, and the concentration of butane in air was 1.5% by volume for all catalysts.

[c] Selectivity at 4% conversion.

(iii) evaporation of the solution on a Schlenk line under vacuum. The precursors were denoted as VPO_{SCP1}, VPO_{LP}, and VPO_{EP}, respectively. These precursors were evaluated as catalysts for the partial oxidation of *n*-butane to maleic anhydride, and the results are shown in Tables 1 and 2. For comparison, the results for typical catalysts prepared by the standard VPA, VPO, and VPD procedures are also shown.

It is apparent that none of the three catalysts requires an activation period to establish the steady-state catalyst performance which is generally associated with vanadium phosphate catalysts (1, 5, 6). During this activation period, it is usual that catalysts derived from crystalline hemihydrate

TABLE 2

Catalytic Performance of Vanadium Phosphate Catalysts[a]

Preparation route	Butane conversion (%)	Selectivity (%)		
		Maleic anhydride	CO	CO_2
VPA[b]	11	51	41	7
VPO[b]	27	52	34	14
VPD[b]	62	64	21	14
VPO_{SCP1}[b]	16	44	30	26
VPO_{SCP2}[c]	30	24	0	76
VPO_{LP}[b]	17	39	23	38
VPO_{EP}[b]	11	40	31	29
VPO_{CoSC}[d]	3.5	31	48	21
VPO_{acacSC}[d]	9.6	39	28	33

[a] Reaction conditions: 400°C, 1.5% *n*-butane in air.

[b] GHSV = 2400 h^{-1}.

[c] GHSV = 3000 h^{-1}.

[d] GHSV = 4070 h^{-1}.

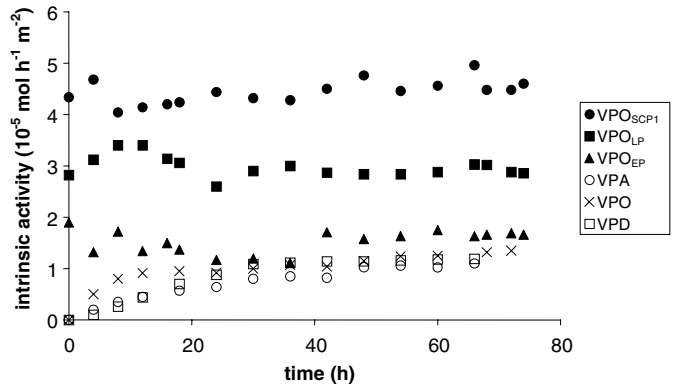

FIG. 2. The intrinsic activity for maleic anhydride (mol h^{-1} m^2) with time on stream. For VPA/VPO/VPD catalysts, GHSV = 1200 h^{-1}; for all other catalysts, GHSV = 2400 h^{-1}.

$VOHPO_4 \cdot 0.5H_2O$ undergo a structural transformation to $(VO)_2P_2O_7$ and $VOPO_4$ phases (5, 6). However, it is clear that, for the precursors VPO_{SCP1}, VPO_{LP}, and VPO_{EP}, this activation period is absent (Fig. 2). The catalysts derived from VPO_{SCP1}, VPO_{LP}, and VPO_{EP} all have low surface areas of 4, 6, and 8 $m^2\ g^{-1}$; respectively, compared with the standard VPO (14 $m^2\ g^{-1}$) and VPD (43 $m^2\ g^{-1}$) materials. The intrinsic activities for these catalysts are shown in both Table 1 and Fig. 2. From these data, it is clear that the catalyst derived from VPO_{SCP1} has a significantly higher intrinsic activity for the production of maleic anhydride. This preparation method was repeated many times, and the enhanced activity was always observed. Interestingly, the catalyst derived from the precursor prepared in liquid CO_2 has an intrinsic activity higher than that for the VPA/VPO/VPD catalysts, whereas the catalyst derived from the sample prepared by evaporation, VPO_{EP}, exhibited an intrinsic activity similar to that for the VPA/VPO/VPD catalysts.

In a further set of experiments, a catalyst was prepared from an isobutanol solution of $VOCl_3$ and H_3PO_4 treated with supercritical CO_2. The material, denoted VPO_{SCP2}, was evaluated as a catalyst, and it is apparent that this material, as compared to VPO_{SCP1} (Tables 1 and 2), is less effective as a catalyst.

Two further catalysts were evaluated and prepared from both the Co-doped isopropanol solution (VPO_{CoSC}) and the acetylacetone-doped isopropanol solution (VPO_{acacSC}). Interestingly, the VPO_{CoSC} catalyst is quite inactive for the oxidation of *n*-butane. The VPO_{acacSC} sample is active but is significantly less so than the catalyst derived from VPO_{SCP1}. The results with the Co-doped sample are particularly interesting, since Co is known to act as a catalyst promoter for the VPA/VPO/VPD-derived catalysts. This, therefore, represents a further significant difference between catalysts derived from crystalline $VOHPO_4 \cdot 0.5H_2O$ and catalysts prepared using supercritical CO_2 as an antisolvent. An analysis of the catalysts prepared using supercritical

CO_2 showed that they contained impurities (Fe, 8000 ppm; Cr, 2000 ppm; Ni, 800 ppm) which are considered to originate from the apparatus used in these initial studies. Hence, the vanadium phosphates prepared in this way may indeed involve multiple promoters, and *these may be present* at nonoptimal levels. This may be a reason for the poor performance of the catalyst containing additional Co, since high concentrations of promoters are known to be less active as catalysts for *n*-butane oxidation to maleic anhydride (4).

The selectivity to maleic anhydride is also compared at 10 and 20% *n*-butane conversion for the catalysts, and these data are given in Table 1. The selectivities to maleic anhydride for the material prepared using supercritical CO_2 as an antisolvent are lower than those to the crystalline vanadium phosphates when compared at the same conversion levels. This, coupled with the higher level of activity, may indicate that, at present, an optimal distribution of the active sites on the catalyst surface has not been achieved.

Catalyst Characterisation

The precursors and the catalysts derived from VPO_{SCP1}, VPO_{SCP2}, VPO_{LC}, VPO_{EP}, VPO_{CoSC}, and VPO_{acacSC} were examined using powder XRD and laser Raman spectroscopy. All the precursors were found to be amorphous by X-ray diffraction, and furthermore no Raman spectra could be obtained from these samples. Following the catalyst evaluation in the microreactor, the VPO_{SCP1}, VPO_{SCP2}, VPO_{CoSC}, and VPO_{acacSC} samples remained amorphous to X-ray diffraction, and, again, no Raman spectra could be obtained. However, the samples derived from precipitation with liquid CO_2 (VPO_{LP}) and from evaporation (VPO_{EP}) were found to have crystallised during the catalyst evaluation in the microreactor. The powder XRD and laser Raman spectra for VPO_{LP} and VPO_{EP} are shown in Fig. 3, and it is apparent that the crystalline material is a mixture of $(VO)_2P_2O_7$ and $VOPO_4$ phases, as was observed in the conventional VPA/VPO/VPD catalysts. It is therefore entirely consistent that the intrinsic activities for the production of maleic anhydride are similar for these catalysts (Fig. 2).

^{31}P NMR spectroscopy confirms the presence of crystalline material (Fig. 4). The spin–echo mapping spectrum of the VPO_{EP} precursor has a signal centred at 1000 ppm which is characteristic of V^{4+}–V^{5+} dimers. The VPO_{EP} precursor has several contributions to the signal: 1000 ppm, which is characteristic of V^{4+}–V^{5+} dimers, 650–600 and 250 ppm, which are due to V^{4+}–V^{5+} dimers associated with V^{5+} sites, and 0 ppm, which is due to V^{5+} sites. Both samples have a single sharp resonance at 0 ppm after catalyst testing which is characteristic of V^{5+}, and ^{31}P MAS NMR was used to resolve the nature of the V^{5+} material present (Fig. 4b). For the VPO_{EP} catalyst, the spectrum is characteristic of δ-$VOPO_4$, with signals at -10 and -21 ppm. The VPO_{LP} material also has the characteristic δ-$VOPO_4$ spectrum but has additional resonances at 27 and 36 ppm, which are a result of V^{5+} microdomains in the catalyst.

The catalysts derived from precipitation using supercritical CO_2 were then examined in further detail. First, the precursors and activated catalysts were examined using TEM, and representative micrographs of these materials are shown in Fig. 5. The VPO_{SCP1} precursor material (Fig. 5a) consists of discrete spherical particles ranging between 75 nm and 5 μm in size, although most lie between 75 nm and 1 μm in diameter. These particles show no diffraction contrast (only thickness contrast) and are very prone to electron beam damage. The activated VPO_{SCP1} catalyst prepared from the isopropanol solution (Fig. 5b) comprises agglomerated spherical particles which show the initial signs of sintering. Several spherical voids, ca. 20 nm in diameter, are usually seen within each particle, arising presumably from the loss of water during activation. Low-dose, high-resolution electron microscopy (HREM) imaging experiments on both the VPO_{SCPI} precursor and the activated catalysts showed no sign of either lattice fringes or nanocrystalline order; only amorphous speckle contrast is seen. Selected area electron diffraction analysis of the precursor and activated catalysts derived from VPO_{SCP1} show them to be amorphous. This is consistent with the fact that the particles show no crystallographic faceting and adopt a minimum surface area (i.e., spherical) morphology. In the VPA/VPO/VPD-derived catalysts, the activation procedure in *n*-butane/air always generates a considerable fraction of crystalline $(VO)_2P_2O_7$, together with some $VOPO_4$ polymorphs (32). These crystalline phases are readily identifiable by powder X-ray diffraction, HREM, and electron diffraction. We consider that the material VPO_{SCP1}, as either the precursor or the activated catalyst, comprises a stable mixed P_2O_5–V_2O_5 glassy phase. This is entirely feasible, since both P_2O_5 and V_2O_5 satisfy Zachariasen's rules for glass formation (40) and are completely miscible. In fact, even heating VPO_{SCP1} in pure N_2 at 750°C for 6 h resulted in the formation of a relatively minor amount (i.e., less than 5 vol%) of nanocrystalline $(VO)_2P_2O_7$. A similar treatment of $VOHPO_4 \cdot 0.5H_2O$ derived from the VPA/VPO/VPD methods would result in complete crystallisation to $(VO)_2P_2O_7$. The precursor VPO_{SCP2}, prepared using isobutanol as solvent, showed a morphology identical to that of VPO_{SCP1} (Fig. 5c). However, in contrast to VPO_{SCP1}, the VPO_{SCP2} material after activation (Fig. 5d) showed the presence of a significant proportion of nanocrystalline $(VO)_2P_2O_7$ that had formed during the catalyst evaluation period. Interestingly, this catalyst was less active for the formation of maleic anhydride. This demonstrates that the alcohol used as solvent can affect the nature of the material prepared using supercritical CO_2 as an antisolvent.

^{31}P spin–echo mapping NMR spectroscopy also confirms that both the precursor and the catalyst prepared from

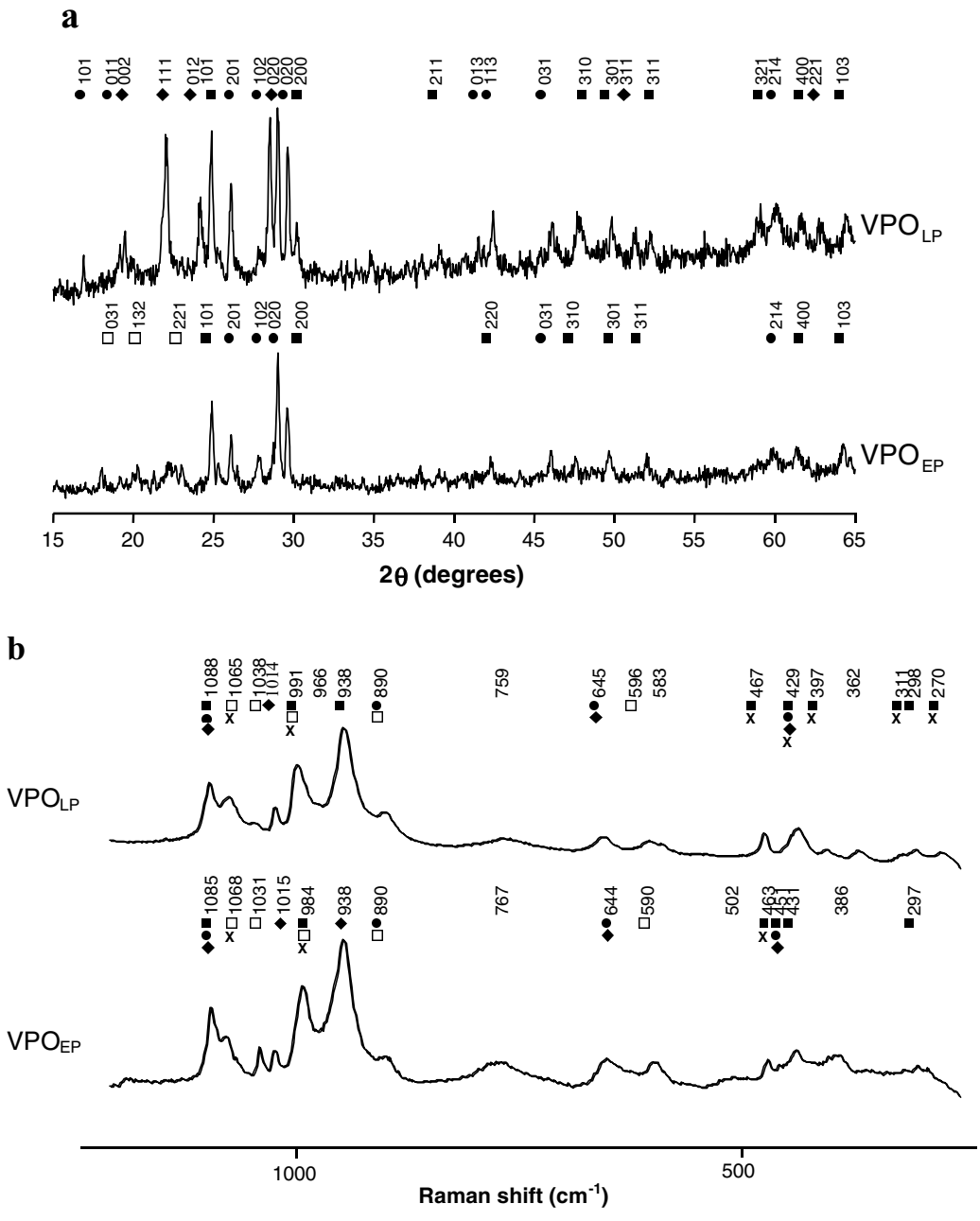

FIG. 3. Characterisation of catalysts derived from VPO_{LP} and VPO_{EP}: (a) XRD and (b) laser Raman spectra. Key: ■, α_{II}-$VOPO_4$; ●, β-$VOPO_4$; □, γ-$VOPO_4$; ◆, δ-$VOPO_4$; X, $(VO)_2P_2O_7$.

VPO_{SCP1} are distinctly different from the conventional $VOHPO_4 \cdot 0.5H_2O$-derived precursors and activated catalysts (Fig. 6). In Fig. 6a, the presence of a high number of V^{4+}–V^{5+} dimers at 1100 ppm are clearly visible. A small contribution from V^{5+} sites at 0 ppm is also observed, and this becomes more pronounced in intensity following catalyst testing (Fig. 6b), which demonstrates that some modification of the material occurred during the catalyst testing. Significantly, in both the precursor and the catalyst derived from VPO_{SCP1}, there is no significant contribution at 2400 ppm, indicating the absence of any crystalline $(VO)_2P_2O_7$ phase.

XPS of the new amorphous VPO_{SCP1} before and after catalyst testing also confirms it to be different from the VPA/VPO/VPD precursors and catalysts. Conventional catalysts based on $(VO)_2P_2O_7$ are known to be significantly enriched with phosphorus at the surface (1, 32). For the amorphous VPO_{SCP1}-derived precursor and activated catalyst, the P/V ratio is closer to unity. Semiquantitative SEM–EDX analysis of the bulk composition was also

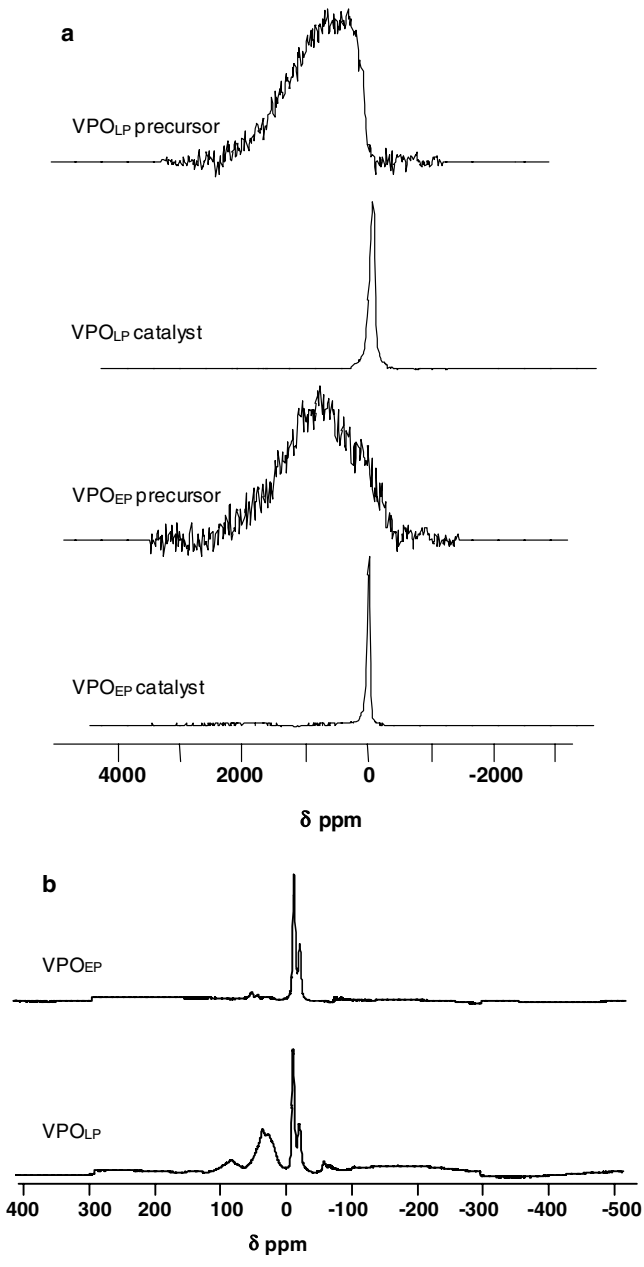

FIG. 4. ^{31}P NMR spectroscopy of the materials derived from both VPO_{LP} and VPO_{EP}. (a) Spin-echo mapping spectra of the precursors and catalysts. (b) MAS spectra of the catalysts.

performed on the VPO_{SCP1} materials. Both the precursor and the activated catalysts are rich in P with bulk P/V ratios in the range $1.2 < P/V < 1.5$. Treatment of VPO_{SCP1} in pure N_2 at 750°C for 6 h caused the P/V ratio to fall to $0.5 < P/V < 0.7$. This latter observation is consistent with previous reports that P and O were preferentially lost from P_2O_5–V_2O_5 glasses when heated (40).

In Fig. 7, the vanadium $L_{2,3}$- and the oxygen K-absorption edge of the totally amorphous catalyst prepared using the new supercritical method (VPO_{SCP1}), a crystalline catalyst prepared using the alcoholic route (VPO), and a supercritical catalyst doped with cobalt (VPO_{CoSC}) are displayed. As indicated, the OK-edge follows directly in photon energy after the vanadium L-edges. The vanadium L-edges can be separated into structures belonging to the $V2p_{3/2} \rightarrow V3d$ (VL_3-edge) and to the $V2p_{1/2} \rightarrow V3d$ (VL_2-edge) transitions, respectively. At the oxygen edge (approximately at photon energies higher than 528 eV), there are contributions from hybridisation of $O2p$ states with vanadium and $O2p$/phosphorus states superimposed. By comparison with reference phosphates, it can be concluded that the first absorption resonances from 529 to 535 eV are mainly contributed by $O2p/V3d$ states, while the strong features above 534 eV mainly arise from hybridisation of oxygen and phosphorus molecular orbitals. In the figure it can be seen that all catalysts exhibit three distinct absorption features at 529.3, 530.8, and 532.4 eV, but their intensity ratios vary. While for the catalysts VPO and VPO_{CoSC} the first resonance is the most intensive, all three resonances are almost equal in intensity for the undoped catalyst VPO_{SCP1}. As mentioned above, this can be interpreted as a significant difference in the V–O bonding situation for the amorphous sample, which seems to be quite unusual for vanadyl pyrophosphate catalysts. The broad resonance around 538 eV, attributed to O/P hybridised electronic states, is most pronounced at the supercritical catalyst VPO_{SCP1} compared to the normalised intensity at the vanadium edge.

Further analysis was subsequently focused on the VL_3-NEXAFS shown for the above-mentioned catalysts VPO_{SCP1}, VPO, and VPO_{CoSC} in Fig. 8. The vanadyl pyrophosphate catalysts show a very detailed absorption structure at the VL_3-edge. Details of the NEXAFS can be interpreted in a framework which relates peak positions to bond lengths (39). Therefore, analysing the different resonances yields direct information about specific vanadium–oxygen bonds present in the catalyst.

At first sight, the three samples show a very similar overall spectral function. The resonance positions obtained by an unconstrained least-squares fit do not differ by more than 0.2 eV (compare also Table 3, where numbers of assumed resonances for VPO_{SCP1} and VPO_{CoSC} are obtained from the fit for VPO). The intensity proportions are quite similar, except for those of the Co-doped catalyst, where the resonance V5 around 517.1 eV is not as dominant as those in the other samples. This can be clearly seen in the distribution of the spectral weights reported in Table 4. Two observations are striking when the totally amorphous catalyst VPO_{SCP1} and the crystalline VPO are compared. First, the resonance V7 at 519 eV, present in both VPO and VPO_{CoSC}, is almost absent in VPO_{SCP1}. Second, the overall shape of the VL_3-absorption edge looks less structured for VPO_{SCP1}. This is expressed by the on-average significantly higher width of the fitting profiles. The broadening of absorption resonances is a well-known phenomenon for amorphous samples compared to crystalline materials and is also observed, for example, with amorphous graphite and

TABLE 3

The Resonance Positions at the VL_3-Edge and the Extracted Bond Lengths for Different Catalysts under *ex Situ* Conditions

Resonance indices	V1	V2	V3	V4	V5	V6	V7
VPO_{SC} Resonance position (eV)	514.42	515.06	515.67	516.45	517.21	517.98	519.05
VPO_{SC} V–O bond length (Å)	2.25–2.26	2.14–2.16	2.04–2.07	1.90–1.96	1.77–1.85	1.63–1.74	1.45–1.59
VPO Resonance position (eV)	514.36	515.94	515.56	516.39	517.16	517.97	519.05
VPO V–O bond length (Å)	2.25–2.26	2.17	2.05–2.08	1.91–1.96	1.78–1.86	1.64–1.75	1.52–1.65
VPO_{CoSC} Resonance position (eV)	514.22	515.90	515.60	516.29	517.01	517.90	518.78
VPO_{CoSC} V–O bond length (Å)	2.27–2.29	2.17–2.18	2.05–2.08	1.93–1.98	1.80–1.88	1.65–1.75	1.49–1.63

Note. Different bond lengths according to assumed models in Ref. (39). For comparison, bond lengths by XRD (42): 2.19–2.20 Å, 2.07–2.08 Å, 1.93–1.95 Å, 1.50–1.52 Å.

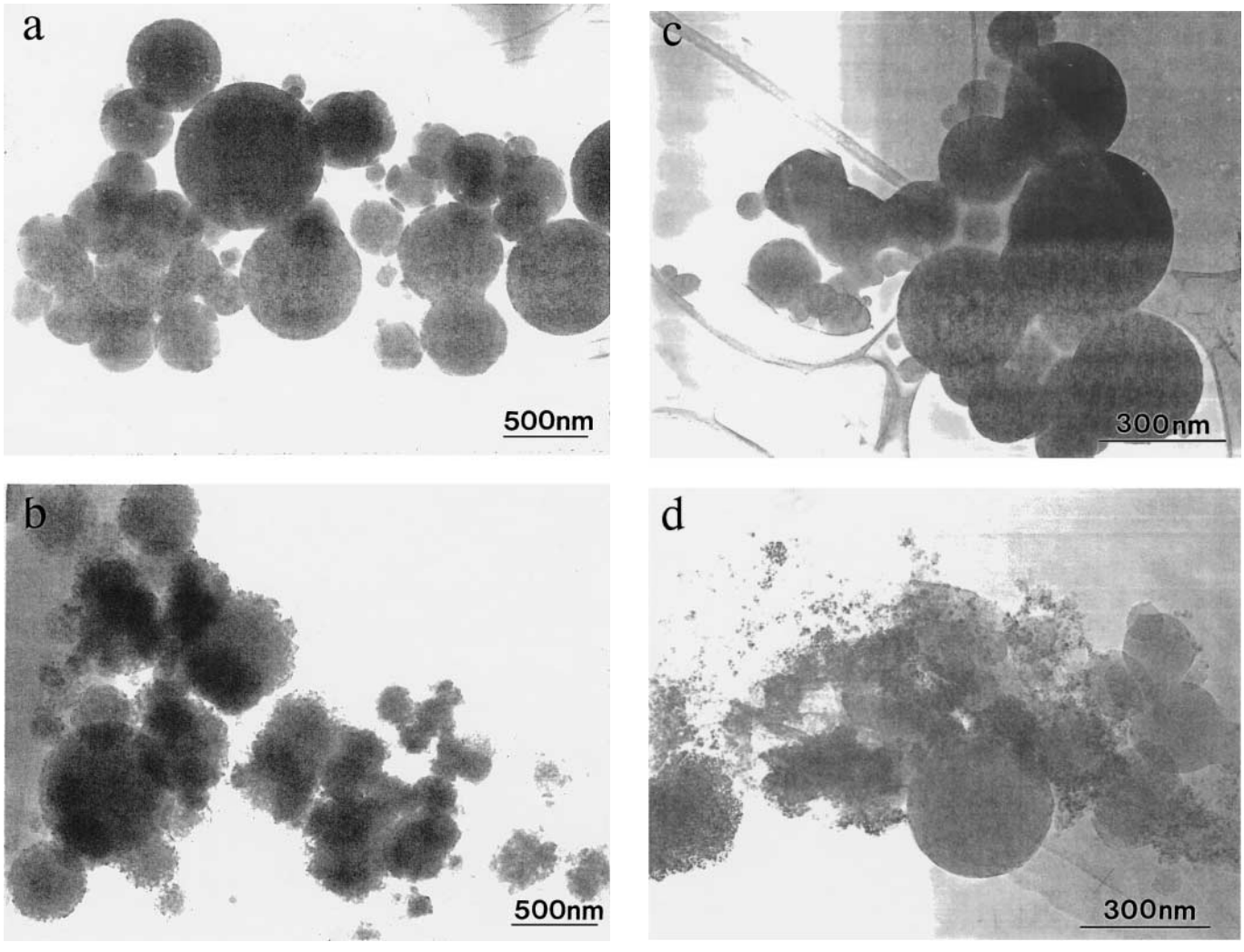

FIG. 5. Transmission electron micrographs of (a) VPO_{SCP1} prior to catalyst testing, (b) VPO_{SCP1} after catalyst testing, (c) VPO_{SCP2} prior to catalyst testing, (d) VPO_{SCP2} after catalyst testing.

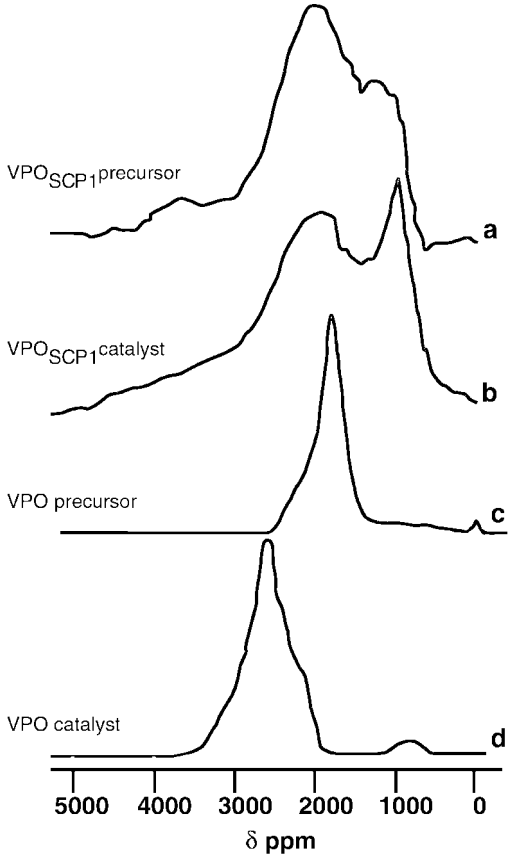

FIG. 6. ^{31}P spin-echo mapping NMR spectroscopy of (a) the VPO$_{SCP1}$ precursor, (b) the VPO$_{SCP1}$ following catalyst testing, (c) a conventional crystalline $VOHPO_4 \cdot 0.5H_2O$ precursor, (d) the activated catalyst derived from (c).

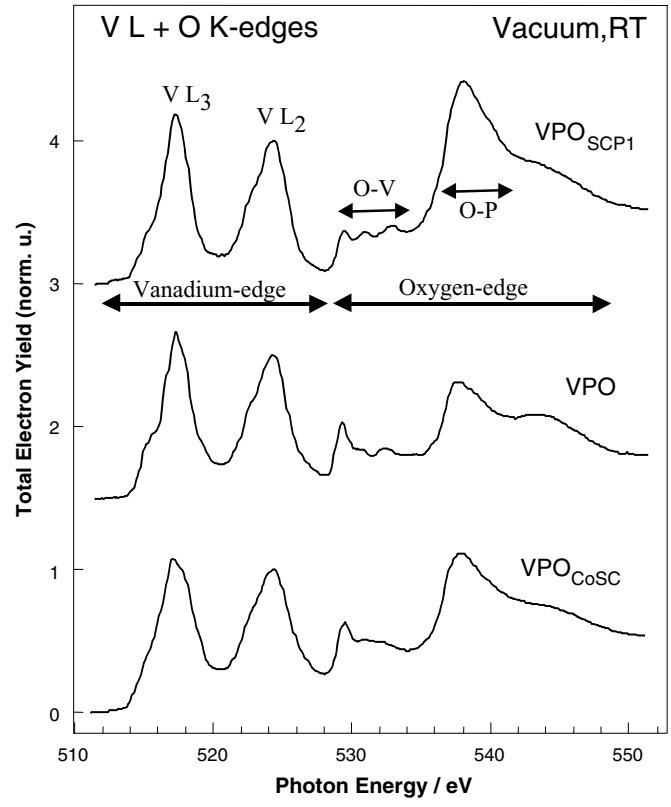

FIG. 7. X-ray absorption spectra at the V$L_{2,3}$- and O K-edges of VPO$_{SCP1}$, VPO, and VPO$_{CoSC}$. Indicated in the figure is a schematic separation in VL- and OK-absorption edges and areas of main contributions by O–V and O–P electronic orbitals. All spectra were normalised on intensity maximum at the VL_2-edge.

HOPG (41). Nevertheless, the NEXAFS is similar, hinting that the undoped catalysts exhibit a very similar local electronic structure in the information depth of approximately 60 Å. In Table 3, energy positions and V–O distances according to the empirical found relationship between the resonance position at the VL_3-edge and the bond length are given (39). Remarkably, for some strong resonances with extracted bond lengths of 1.7 and 1.8 Å (V5 and V6, respectively), no equivalent in the geometric vanadyl pyrophosphate structure obtained by XRD measurements (42) can be found. For comparison, these are also reported in Table 3.

TABLE 4

Spectral Weights of Resonances V1–V8 for VPO$_{SCP1}$, VPO, and VPO$_{CoSC}$ According to the Fit Displayed in Fig. 8

VPO$_{SCP1}$		VPO		VPO$_{CoSC}$	
Resonances	Percentage	Resonances	Percentage	Resonances	Percentage
V1	1	V1	0	V1	0
V2	5	V2	5	V2	5
V3	7	V3	10	V3	8
V4	11	V4	7	V4	9
V5	43	V5	45	V5	24
V6	22	V6	15	V6	33
V7	5	V7	12	V7	13
V8	6	V8	6	V8	8

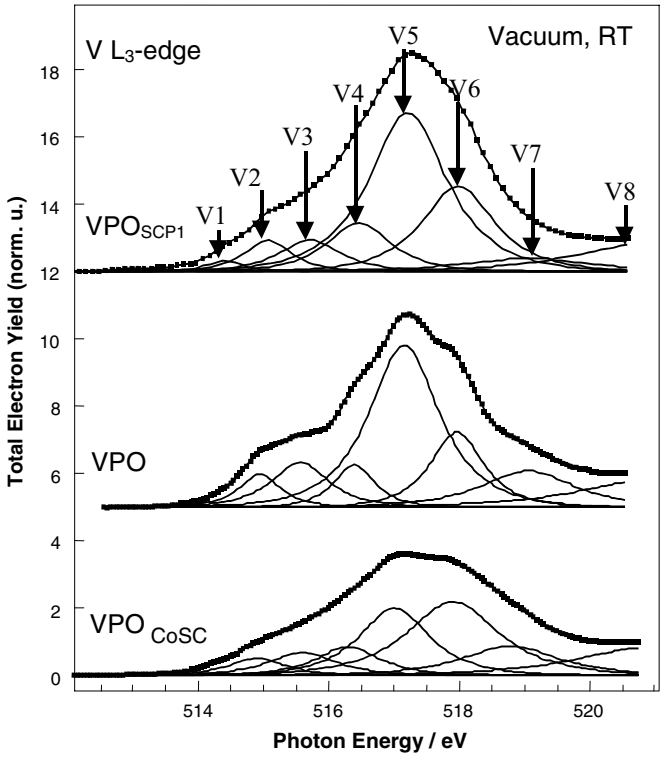

FIG. 8. NEXAFS at the VL_3-edge of VPO_{SCP1}, VPO, and VPO_{CoSC}. The fit profiles used are shown and labelled according to their energetic ordering.

In addition to these *ex situ* XAS investigations under vacuum, *in situ* experiments were also performed under *n*-butane oxidation conditions with the totally amorphous material VPO_{SCP1}. The set of spectra at the VL_3-edge under these conditions can be found in Fig. 9. It is easy to observe that the NEXAFS changes dramatically ((a)→(b)). The overall spectral weight is shifted to lower photon energies. This shift is caused by a 15% decrease of the intensity of resonance V5. The spectral weight of V4 is strongly increased by a factor of 2.5. This change is partially reversible by switching to pure oxygen ($P = 0.4$ mbar, $T = 400°C$), which causes a decrease of V4 and an increase of V5 ((b)→(c)). This shows that the surface of the catalyst is highly flexible, and its response to the applied conditions becomes visible with *in situ* XAS.

It is well known from low-resolution X-ray absorption spectra of vanadium compounds that the position of the maximum of the VL_3-edge can be directly correlated to the oxidation state (43–45). To transfer this relationship to the high-resolution spectra reported in Fig. 8 the momentum ($E_{centre} = \int E \cdot TEY(E)\, dE$) of the area-normalised spectral distribution at the VL_3-edge was calculated. By calculating E_{centre} for reference compounds with a known oxidation state (V^{5+}: $VOPO_4 \cdot 2H_2O$, β-$VOPO_4$; $V4^+$: $VOHPO_4 \cdot 0.5H_2O$) and for catalysts with an independently determined oxidation state (by titration and from the position of the prepeak at the V*K*-edge (46)) a linear correlation between E_{centre} and the average oxidation state of the material was found (Fig. 10). The oxidation state of the VPO_{SCP1} under different reaction conditions can then be determined by this method. It was found that starting from an average oxidation state (V_{ox}) of 4.03 at room temperature (A) the catalyst is then reduced ($V_{ox} = 3.79$) under the butane oxidation conditions applied (B). Heating in pure oxygen (C) results in minor reoxidation ($V_{ox} = 3.85$). The easy reduction of the catalyst observed under these conditions may be one reason for the comparatively low selectivity to maleic anhydride of these materials.

The mass spectra of the gas phase were monitored simultaneously (Fig. 11), and this indicates an *n*-butane conversion of 3.5%, detectable by the decrease of the intensity of mass fragments $m/e = 43$ and $m/e = 41$, after the reaction temperature of 400°C is reached. Under similar reaction conditions, a conversion of around 5% is observed for a crystalline VPO catalyst, although it must be noted that the crystalline VPO catalyst has a significantly higher surface area. Consequently, this *in situ* experiment confirms the increased intrinsic activity of the VPO_{SCP1} material.

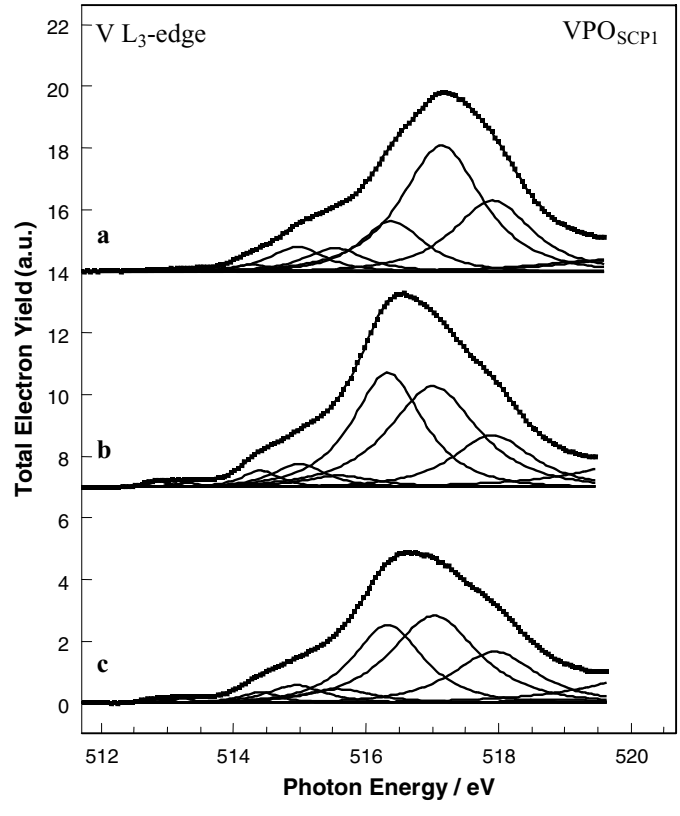

FIG. 9. *In situ* NEXAFS of VPO_{SCP1} under different reaction conditions: (a) at room temperature in a mixture of *n*-butane/helium/oxygen (1.2/78.8/20) at a total pressure of 2 mbar, (b) in the same reaction mixture at 400°C, (c) in pure oxygen (0.4 mbar) at 400°C. Also shown are the fit profiles used.

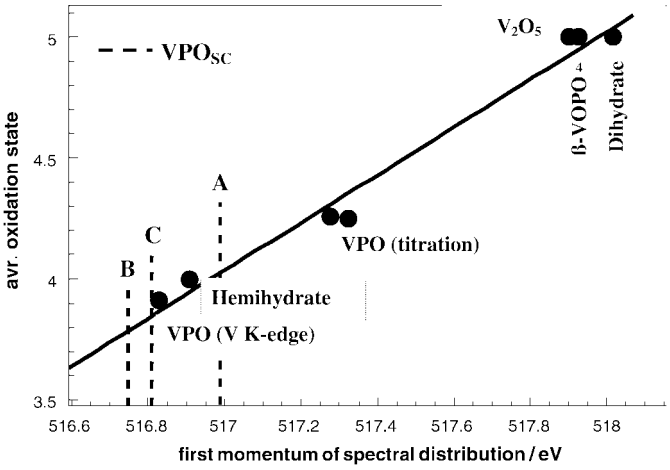

FIG. 10. Correlation between the first momentum, E_{centre}, of the spectral distribution at the VL_3-edge and the average oxidation state of the material. E_{centre} is shown for reference compounds with a known oxidation state (●) and the linear relation (solid line) obtained by regression. E_{centre} of VPO$_{SCP1}$ at different reaction conditions. A–C, as described in Fig. 9, are indicated by dashed lines.

Even if the overall conversion obtained under these low-pressure conditions is much less than that observed under atmospheric pressure, the relation between the conversions obtained with VPO$_{SC}$ and VPO is quite similar to those indicated in Table 1. Initially, on heating, a release of water is detected, which may cause some of the dramatic changes in the VL_3-NEXAFS. Simultaneously CO_2 can be observed. The yield of CO_2 decreases when the sample is maintained under reaction conditions for 55 min, while the *n*-butane conversion remains constant. This might be an indication of the partial oxidation reaction to maleic anhydride, which could not be detected directly by mass spectroscopy in our experiments, perhaps due to condensation problems in unheated parts of the capillary line.

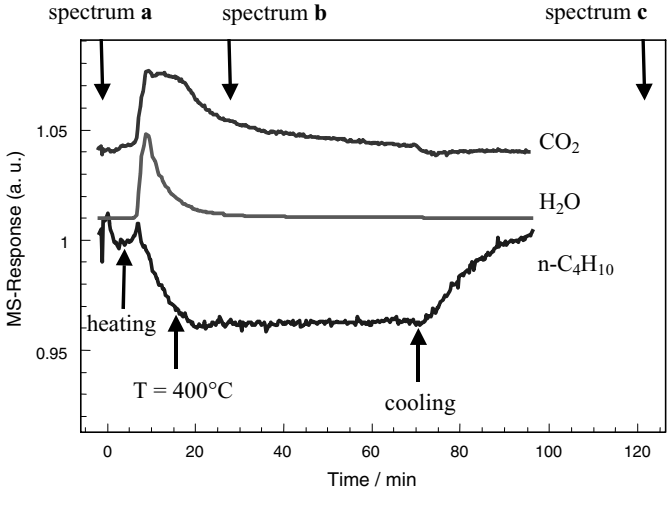

FIG. 11. Monitored mass spectra of *n*-butane, H_2O, and CO_2 during heating of VPO$_{SCP1}$. Reaction conditions: *n*-butane/He/O_2 = 12/78.8/20, at a total pressure of 2 mbar; temperature ramped from room temperature to 400°C, held for 55 min, then cooled back to room temperature. The arrows indicate the point at which the NEXAFS spectra shown in Fig. 9 were obtained.

DISCUSSION

Rapid precipitation of a vanadium phosphate from an alcohol solution using supercritical CO_2 as an antisolvent provides a preparation route for an amorphous vanadium phosphate. It is clear that both the alcohol and the method of solvent removal are important if the amorphous material is to retain its amorphous character under the reaction conditions. When isopropanol is used as the solvent and supercritical CO_2 is used as the antisolvent, the resulting amorphous VPO material remains amorphous under the reaction conditions. Indeed, subjecting the material to aggressive conditions known to crystallise vanadium phosphate to form well-crystalline $(VO)_2P_2O_7$ (750°C, in flowing He, >8 h) only leads to a very small amount of crystallisation. However, if the solvent is changed to isobutanol, the amorphous material forms some microcrystalline domains of $(VO)_2P_2O_7$ during the catalyst testing, and the material is less active for the selective formation of maleic anhydride. The use of liquid CO_2, in place of supercritical CO_2, also produces an amorphous VPO precursor, but this partially crystallises to both $(VO)_2P_2O_7$ and $VOPO_4$ during the catalyst test period. The removal of the solvent by evaporation is another route that produces an amorphous precursor, but, again, this crystallises during the catalyst test period. It is possible that using supercritical CO_2 affords the most rapid precipitation and that the nature of the alcohol solvent can also influence the precipitation process. It is interesting to note that the addition of acetylacetone to the isopropanol solvent and the use of supercritical CO_2 as an antisolvent produce an amorphous VPO material that remains amorphous after being used as a catalyst. However, in this case the amorphous VPO material is less active on the basis of intrinsic activity. We have previously shown, for catalysts derived from crystalline $VOHPO_4 \cdot 0.5H_2O$, that the addition of low levels of ketones can significantly influence the catalytic performance (47), and it is possible that this effect is also maintained for this catalyst preparation method.

At the present stage of this work, the major problems that require attention concern the surface area of the amorphous material, the selectivity to maleic anhydride, and the levels of adventitious promoters that are present due to the preparation method used. To date, surface areas typically in the range 2–7 $m^2\ g^{-1}$ are readily achievable. Hence, although the intrinsic activity is higher than that of conventional catalysts, the overall reaction performance is not enhanced. In a future phase of this work, it will be important to devise methods of enhancing the surface area to

ca. 30 $m^2\ g^{-1}$ to take full advantage of the high intrinsic activity. In addition, the selectivity to maleic anhydride is somewhat lower than that observed for the current unpromoted conventional VPA, VPO, and VPD catalysts. This is considered to be due to nonoptimal site isolation on the surface of the new amorphous vanadium phosphates and can be addressed by modifying the surface V/P atomic ratio. However, the low selectivities may also be due to the levels of Fe, Cr, and Ni that are present acting as nonselective catalysts. It may also be important to prevent the reduction observed under *n*-butane oxidation conditions which is observed by the *in situ* NEXAFS investigation and to stabilise the oxidation state close to V^{4+}.

Using two complementary techniques to study the oxidation state of the vanadium in the bulk (by ^{31}P spin-echo mapping NMR) and at the surface (by NEXAFS) allows the structure–function analysis of the system, with respect to geometric and electronic structures, to be elucidated. In contrast to well-ordered, crystalline systems where these properties are linked together, the amorphous microstructure may allow for independent control of geometric and electronic structures by introducing a variable polyhedra lining such as that in glasses. A new functional model for this catalyst could be proposed with the vanadium phosphate providing a well-crystalline, stable, solid matrix (site isolation) for electronically variable disordered grains of a very similar chemical nature which carry the active sites. Hence, attempts must be made to independently control electronic and geometric structures by varying the gas-phase chemical potential to allow assessments of the quality of a given material (based on testing conditions with fixed feed conditions).

The novel amorphous VPO material, prepared by precipitation with supercritical CO_2 as an antisolvent, demonstrates two clear differences with respect to the well-studied crystalline vanadium phosphate catalysts derived from $VOHPO_4 \cdot 0.5H_2O$. First, VPO_{SCP1} does not require an extensive pretreatment time in the reactor. Stable catalytic performance is attained, and maintained for over 100 h, as soon as the catalyst reaches the required operating temperature. In contrast, catalysts derived from $VOHPO_4 \cdot 0.5H_2O$ always require 24–72 h in the microreactor under the reaction conditions to achieve a stable catalytic performance (1, 5, 6, 32). It is known that, during this period, the catalyst structure is established and the $VOHPO_4 \cdot 0.5H_2O$ topotactically transforms to $(VO)_2P_2O_7$ by either a direct pathway or an indirect route involving δ-$VOPO_4$ (6). Additionally, $VOPO_4$ phases are immediately formed, and the active sites for the selective oxidation of *n*-butane to maleic anhydride are progressively generated on the surface of the crystallites with a specific dispersion of V^{5+} sites. Second, the amorphous VPO_{SCP1} is more active than catalysts derived from $VOHPO_4 \cdot 0.5H_2O$ on the basis of intrinsic activity (mol maleic anhydride produced/m^2/h). Indeed, the VPO_{SCP1}-derived material remains amorphous during the reaction period and maintains this enhanced activity (Fig. 2). This study therefore demonstrates that a wholly amorphous VPO material can act as an effective catalyst, and this is, perhaps, the most important observation from this study.

A number of previous studies (5, 6, 9–11, 14–29) have suggested that amorphous VPO material can play an important role in the selective oxidation of *n*-butane. Many studies have suggested that an amorphous overlayer on the crystalline VPO subsurface may be the active surface for this reaction (5, 6, 15, 18, 19, 26–29). This has also been observed on related vanadium carbide catalysts for butane oxidation (21). It is generally acknowledged that the transformation from well-crystalline $VOHPO_4 \cdot 0.5H_2O$ to the final active catalysts can involve both the formation and the transformation of amorphous material. This was first clearly demonstrated in our *in situ* laser Raman spectroscopy study of the pretreatment step of catalyst preparation (5). A key observation was that the selective oxidation of *n*-butane to maleic anhydride was only observed to commence following the formation of the amorphous vanadium phosphate material. The detailed combined microscopic and spectroscopic studies of this pretreatment stage also confirmed the formation of significant quantities of amorphous material (6).

Additional evidence in support of the proposal that the surface layer of the crystallites of vanadium phosphate is significantly different from the bulk structure is provided by the following observations: (i) X-ray photoelectron spectroscopy (1) consistently shows phosphorus enrichment in the surface layers ($P:V \geq 1.5$), indicating that the surface is significantly different from the bulk structure of the crystallites. Fully crystalline structures of $(VO)_2P_2O_7$ and $VOPO_4$ would not be able to provide this degree of phosphorus enrichment. Furthermore, the phosphorus enrichment is enhanced during the transformation of the precursor $VOHPO_4 \cdot 0.5H_2O$ to the final catalyst. (ii) Catalysts prepared from $VOHPO_4 \cdot 0.5H_2O$ prepared by different routes are observed to give very different relative compositions of $(VO)_2P_2O_7$ and $VOPO_4$ phases, as determined by microscopy, diffraction, and spectroscopy (32), but the catalysts will generally have very similar intrinsic activities for maleic anhydride production. This suggests that these different composition catalysts all exhibit the same active sites on the surface, although the bulk structures are different, which is also supported in the present study by the similar NEXAFS of the fully amorphous and the crystalline catalyst. (iii) In the present study, the assumed resonance-position bond-length relationship gives a high contribution of bond lengths which do not fit to the geometric structure of crystalline vanadyl pyrophosphate obtained by XRD. (iv) The Co promoter for a vanadium phosphate

catalyst, prepared using the VPO route, was found to phase-segregate to, and stabilise, the amorphous material. Co was not found to be present (to the detectability limit of EDS) in the crystalline $(VO)_2P_2O_7$, yet the intrinsic activity of the Co-containing catalyst was enhanced by a factor of 3. This indicates that Co promotes the catalytic performance of the amorphous material derived from this preparation method. It is interesting to note that Co does not have this effect on the amorphous vanadium phosphate catalysts prepared using supercritical CO_2 as an antisolvent (29), at least at the concentration investigated in this study. (v) Oxidation of $(VO)_2P_2O_7$ has been shown to enhance the selectivity to maleic anhydride and to oxidise the surface of the catalyst (22, 28). This oxidation treatment also correlates with an increase in the depth of the amorphous overlayer as observed on edge on the $(VO)_2P_2O_7$ crystallites viewed using very low-illumination transmission electron microscopy (48).

In contrast, a number of researchers have concluded either that the amorphous material is detrimental to catalyst performance (8–11, 22) or that the amorphous material is a transient phase and that, following extensive reaction, only wholly crystalline VPO material was present (8–11). Guliants *et al*. (9–11), in particular, concluded that the amorphous layer terminating the (200) planes of $(VO)_2P_2O_7$ observed in fresh catalysts was not observed in equilibrated catalysts obtained after many days of reaction. They concluded, in agreement with Albonetti *et al*. (16) and Ebner and Thompson (8), that the best catalytic performance was obtained for catalysts containing only $(VO)_2P_2O_7$ with the highest degree of stacking order. In addition, these researchers considered that $VOPO_4$ phases were detrimental to the catalyst performance. Indeed, Volta and co-workers (49) have shown that pure $VOPO_4$ phases were less selective for maleic anhydride than for $(VO)_2P_2O_7$. However, a number of studies have shown that a combination of $VOPO_4$ phases, together with $(VO)_2P_2O_7$, could give enhanced catalyst performance (22, 50, 51). There remains, therefore, a considerable amount of debate concerning the nature of the active sites in vanadium phosphate catalysts, the preferred composition of the catalyst, and the role of the amorphous material. One of the major problems preventing progress in this debate was that, in all these previous attempts to unravel the complexity of the role of the amorphous material, the catalysts all contained substantial quantities of crystalline phases in addition to the amorphous material.

In addition, all the evidence presented from detailed transmission electron microscopy studies concerning either the presence or the absence of amorphous overlayers must be viewed with great care. We consider that the presence of an amorphous overlayer on $(VO)_2P_2O_7$, as noted in many studies (9–11, 15, 18, 19, 23, 24), may result from a combination of one or more of the following processes: (i) exposure of the crystalline surfaces to the reactor feed producing amorphous material *in situ*, (ii) electron beam damage of the $(VO)_2P_2O_7$ crystallites (which are known to completely amorphise after 20–30 s under typical electron beam irradiation conditions in the microscope), and/or (iii) preferential electron beam sensitivity of a crystalline surface layer (e.g., $VOPO_4$, which is known to completely amorphise in a few seconds in the electron beam of the microscopy) (33). It is therefore not possible, with transmission electron microscopy alone, to determine unequivocally whether the presence of a surface amorphous layer is simply an artefact due to beam damage or is, indeed, the genuine catalytically active phase. However, in the present study, the case is very clear. An amorphous VPO catalyst was prepared which retained its amorphous nature throughout the reactor studies. Furthermore, the amorphous material required no activation period and was more active, on a surface area basis, than the *crystalline* counterparts. Hence, the present study shows that amorphous VPO_{SCP1} materials are effective catalysts and require further study at this time. At this stage, it is not possible to determine whether the amorphous VPO material, prepared using supercritical CO_2 as an antisolvent, is similar to either the material observed during the transformation of $VOHPO_4 \cdot 0.5H_2O$ to $(VO)_2P_2O_7$ (5, 6) or the amorphous layers observed supported on $(VO)_2P_2O_7$ crystallites (9–11), although the similarity of the VL_3-NEXAFS suggests a close relationship. On the basis of this study, the key matter for debate is not whether the catalysts derived from $VOHPO_4 \cdot 0.5H_2O$ are wholly crystalline $(VO)_2P_2O_7$ or whether an amorphous layer supported on $(VO)_2P_2O_7$ is the active surface in these catalysts. Rather, it is crucial to determine the nature of the active site (e.g., V^{4+}–V^{5+} dimers, isolated V^{4+} and V^{5+} microdomains as observed by ^{31}P spin-echo mapping) to prepare catalysts with a high density of such sites whilst simultaneously maintaining site isolation to ensure high selectivity to maleic anhydride. Our study suggests that amorphous VPO catalysts may provide one route forward in identifying the optimal vanadium phosphate catalyst.

ACKNOWLEDGMENTS

The authors thank Su Sajip for preliminary electron microscopy studies. In addition, we thank the EPSRC for financial support and the BESSY staff for their continual support during the XAS measurements at the synchrotron in Berlin.

REFERENCES

1. Centi, G., Ed., Vanadyl pyrophosphate catalysts, *in* "Catalysis Today," Vol. 16, Part 1, Elsevier, Amsterdam, 1993.
2. Bordes, E., *Catal. Today* **1**, 499 (1987).
3. Centi, G., Trifiro, F., Busca, G., Ebner, J., and Gleaves, J., *Faraday Discuss*. **87**, 215 (1989).
4. Hutchings, G. J., *Appl. Catal*. **72**, 1 (1992).
5. Hutchings, G. J., Desmartin Chomel, A., Olier, R., and Volta, J. C., *Nature* **368**, 41 (1994).

6. Kiely, C. J., Burrows, A., Hutchings, G. J., Bere, K. E., Volta, J. C., Tuel, A., and Abon, M., *Faraday Discuss*. **105**, 103 (1996).
7. Centi, G., *Catal. Today* **16**, 1 (1993).
8. Ebner, R., and Thompson, M. R., *Catal. Today* **16**, 51 (1993).
9. Guliants, V. V., Benziger, J. B., Sundaresan, S., Yao, N., and Wachs, I. E., *Catal. Lett*. **32**, 379 (1995).
10. Guliants, V. V., Benziger, J. B., Sundaresan, S., Wachs, I. E., Jehng, J. M., and Roberts, J. E., *Catal. Today* **28**, 275 (1996).
11. Guliants, V. V., Holmes, S. A., Benziger, J. B., Heaney, P., Yates, D., and Wachs, I. E., *J. Mol. Catal. A* **172**, 265 (2001).
12. Coulston, G. W., Bare, S. R., Kung, H., Birkeland, K., Bethke, G. K., Harlow, R., Herron, N., and Lee, P. L., *Science* **275**, 191 (1997).
13. Gleaves, J. T., Ebner, J. R., and Knechler, T. C., *Catal. Rev. Sci. Eng*. **30**, 49 (1988).
14. Thompson, M. R., Hess, A. C., Nicholas, J. B., White, J. C., Anchell, J., and Ebner, J. R., *Stud. Surf. Sci. Catal*. **82**, 167 (1994).
15. Berndt, H., Buker, K., Martin, A., Bruckner, A., and Lucke, B., *J. Chem. Soc., Faraday Trans*. **91**, 725 (1995).
16. Albonetti, S., Cavani, F., Trifiro, F., Venturoli, P., Calestani, G., Granados, M. L., and Fierro, J. L.G., *J. Catal*. **160**, 52 (1996).
17. Zeyss, S., Wendt, G., Hallmeier, K. H., Szargan, R., and Lippold, G., *J. Chem. Soc., Faraday Trans*. **92**, 3273 (1996).
18. Bruckner, A., Martin, A., Steinfeldt, N., Wolf, G. U., and Lucke, B., *J. Chem. Soc., Faraday Trans*. **92**, 4257 (1996).
19. Bruckner, A., Kubias, B., and Lucke, B., *Catal. Today* **32**, 215 (1996).
20. Cheng, W. H., and Wang, W., *Appl. Catal. A* **156**, 57 (1997).
21. Meunier, F., Delporte, P., Heinrich, B., Bouchy, C., Crouzet, C., Phamhuu, C., Panissod, P., Leroud, J. L., Mills, P. L., and Ledoux, M. J., *J. Catal*. **169**, 33 (1997).
22. Aitlachgar, K., Tuel, A., Brun, M., Herrmann, J. M., Krafft, J. M., Martin, J. R., Volta, J. C., and Abon, M., *J. Catal*. **177**, 224 (1998).
23. Bruckner, A., Martin, A., Kubias, B., and Lucke, B., *J. Chem. Soc., Faraday Trans*. **94**, 2221 (1998).
24. Martin A., Wolf, G. U., Steinike, U., and Lucke, B., *J. Chem. Soc., Faraday Trans*. **94**, 2227 (1998).
25. Delichere, P., Bere, K. E., and Abon, M., *Appl. Catal. A* **172**, 295 (1998).
26. Ruitenbeck, M., van Dillen, A. J., Barbon, A., van Faassen, E. E., Koningsberger, D. C., and Geus, J. W., *Catal. Lett*. **55**, 133 (1998).
27. Ruiz, P., Bastians, Ph., Caussin, L., Reuse, R., Daza, L., Acosta, D., and Delmon, B., *Catal. Today*. **16**, 99 (1993).
28. Morishige, H., Tamaki, J., Msura, N., and Yamazoe, N., *Chem. Lett*. 1513 (1990).
29. Sajip, S., Rhodes, C., Bartley, J. K., Burrows, A., Kiely, C. J., and Hutchings, G. J., *in* "Catalytic Activation and Functionalisation of Light Alkanes" (E. G. Derouane, Ed.), p. 429. Kluwer Academic, Dordrecht/Norwell, MA, 1998.
30. Stefani, G., and Fontana, P., US Patent 4181628, 1980.
31. Hutchings, G. J., Bartley, J. K., Webster, J. M., Lopez-Sanchez, J. A., Gilbert, D. J., Kiely, C. J., Carley, A. F., Howdle, S. M., Sajip, S., Caldarelli, S., Rhodes, C., Volta, J. C., and Poliakoff, M., *J. Catal*. **197**, 232 (2001).
32. Kiely, C. J., Burrows, A., Sajip, S., Hutchings, G. J., Sananes, M. T., Tuel, A., and Volta, J. C., *J. Catal*. **162**, 31 (1996).
33. Li, J., Lashier, M. E., Schrader, G. L., and Gerstein, B. C., *Appl. Catal*. **38**, 83 (1988).
34. Sananes, M. T., Tuel, A., and Volta, J. C., *J. Catal*. **145**, 251 (1994).
35. Biggs, D., and Seah, M. P., Eds., *in* "Practical Surface Analysis," Vol. 1. Wiley, Chichester, 1990.
36. Hävecker, M., Knop-Gericke, A., Schedel-Niedrig, Th., and Schlögl, R., *Angew. Chem*. **110**, 2049 (1998); *Int. Ed*. **37**, 206 (1998).
37. Knop-Gericke, A., Hävecker, M., Schedel-Niedrig, Th., and Schlögl, R., *Topics Catal*. **15**, 27 (2001).
38. Sawhney, K. J. S., Senf, F., Scheer, M., Schäfer, F., Bahrdt, J., Gaupp, A., and Gudat, W., *Nucl. Instr. Meth. A* **390**, 395 (1997).
39. Hävecker, M., Knop-Gericke, A., Mayer, R. W., Bluhm, H., and Schlögl, R., *J. Electron. Spectrosc. Relat. Phenom.*, in press.
40. Zachariasen, W. H., *J. Am. Chem. Soc*. **54**, 3841 (1932).
41. Comelli, G., Stöhr, J., Robinson, C. J., and Jark, W., *Phys. Rev. B* **38**, 7511 (1988).
42. Nguyen, P. T., Hoffmann, R. D., and Sleight, A. J., *Mater. Res. Bull*. **30**, 1055 (1995).
43. Taftø, J., and Kravinek, O. L., *Phys. Rev. Lett*. **48**, 560 (1982).
44. Abbate, M., Pen, H., Czyzyk, M. T., de Groot, F. M. F., Fuggle, J. C., Ma, Y. J., Chen, C. T., Sette, F., Fujimori, A., Ueda, Y., and Kosuge, K., *J. Electron Spectrosc. Relat. Phenom*. **62**, 185 (1993).
45. Chen, J. G., *Surf. Sci. Rep*. **30**, 1 (1997).
46. Wong, J., Lytle, F. W., Mesmer, R. P., and Maylotte, D. H., *Phys. Rev. B* **30**, 5596 (1984).
47. Bartley, J. K., Wells, R. P. K., and Hutchings, G. J., *J. Catal*. **195**, 423 (2000).
48. Sajip, S., Ph.D. thesis, University of Liverpool, 1998.
49. Ben Abdelouahab, F., Olier, R., Ziyad, M., and Volta, J. C., *J. Catal*. **134**, 151 (1992).
50. Aitlachgar, K., Abon, M., and Volta, J. C., *J. Catal*. **171**, 383 (1997).
51. Hutchings, G. J., and Higgins, R., *J. Catal*. **162**, 153 (1996).